ACS Macro Letters

Letter

Cite This: ACS Macro Lett. 2018, 7, 1051−1055

pubs.acs.org/macroletters

Location of Imbibed Solvent in Polymer-Grafted Nanoparticle Membranes

Eileen Buenning,[†] Jacques Jestin,[‡] Yucheng Huang,[§] Brian C. Benicewicz,[§] Christopher J. Durning,[†] and Sanat K. Kumar*[,†]

[†]Department of Chemical Engineering, Columbia University, New York, New York 10027, United States

[‡]CEA Saclay, Lab Léon Brillouin, F-91191 Gif Sur Yvette, France

[§]Department of Chemistry and Biochemistry, University of South Carolina, Columbia, South Carolina 29201, United States

Supporting Information

ABSTRACT: Membranes made purely from nanoparticles (NPs) grafted with polymer chains show increased gas permeability relative to the analogous neat polymer films, with this effect apparently being tunable with systematic variations in polymer graft density and molecular weight. To explore the structural origins of these unusual transport results, we use small angle scattering (neutron, X-ray) on the dry nanocomposite film and to critically examine in situ the structural effects of absorbed solvent. The relatively low diffusion coefficients of typical solvents ($\sim 10^{-12}$ m^2/s) restricts us to thin films (≈ 1 μm in thickness) if solute concentration profiles are to equilibrate on the 1 s time scale. The use of such thin films, however, renders them as weak scatterers. Inspired by our nearly two decades old previous work, we address these conflicting requirements through the use of a custom designed flow cell, where stacks of 10 individual ≈ 1 μm thick supported films are used, while ensuring that each film is individually exposed to solvent vapor. By using isotopically labeled solvents, we study the solvent distribution within the film and show surprisingly that the solvent homogeneously swells the polymer under all conditions that we examined. These results are not anticipated by current theories, but they suggest that, at least under some conditions, the free volume increases due to the grafting of chains to nanoparticles is apparently distributed isotropically in these materials.

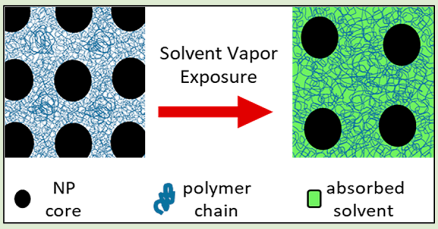

Polymer nanocomposites (PNCs) are attractive due to their ability to combine low-cost, lightweight polymers with inorganic nanoparticles (NPs) to create materials with tunable mechanical, optical, and transport properties.[1] While the macroscopic properties of these hybrids are strongly influenced by the multiscale NP organization, the intrinsic immiscibility between the inorganic (hydrophilic) NPs and the organic (hydrophobic) polymer makes it difficult to achieve and control this organization.[2] Covalently linking polymers to the NPs to create one-component grafted nanoparticles (GNP) circumvents many of these problems.[2−4] Recently we showed that GNP membranes, with no free polymer ("matrix free"), exhibited remarkable increases in gas/condensable solute permeabilities relative to that of the neat polymer.[5] In particular, solute permeability displayed a peak as a function of graft molecular weight, M_n, at a fixed grafting density, σ. To explain this behavior, we postulated that the grafted chains must distort to completely fill the interstitial voids between the NPs while maintaining an essentially constant polymer density due to the incompressibility of the polymer melt.[5−7] When a penetrant molecule is placed in these brushes, the material swells and the chains assume more favored, undistorted conformations. While these arguments rationalize the sources of increased permeability, they do not shed light on where the solute molecules are placed, namely, whether they are present (i) isotropically in the grafted layer or (ii) in preferential locations in the medium.

Scaling theories on spherical brushes[8−11] in solution and simulations[12−16] suggest that, for sufficiently high graft densities, the region near the NP surface is impenetrable to solvent molecules, since the polymer chains are highly stretched. With increasing distance from the surface, however, the monomer density decreases allowing for solvent penetration. Therefore, we expect that solvent density must be dependent on distance from the NP. These arguments would strongly suggest that scenario (ii) above would best describe solute placement in these GNP membranes.

In this work, we study the solvent distribution in situ as a function of ethyl acetate (EtAC) loading in poly(methyl acrylate) (PMA) grafted silica NPs (M_n = 53000g/mol, $Đ$ = 1.16, σ = 0.43 chains/nm^2) using both small-angle X-ray (SAXS) and neutron (SANS) scattering. The Flory−Huggins parameter, χ, of EtAC and PMA is $\approx 0.40-0.43$,[17,18] that is, it is a good solvent. Due to relatively low neutron flux, SANS experiments are ideally performed with thick samples (mm−cm thickness) to minimize counting time while yielding good

Received: June 26, 2018
Accepted: August 8, 2018

Downloaded via UNIV OF SOUTH CAROLINA COLUMBIA on September 12, 2018 at 16:12:13 (UTC).
See https://pubs.acs.org/sharingguidelines for options on how to legitimately share published articles.

statistics. For our swelling experiments, however, sample thicknesses, L, are constrained by the times required for film equilibration with respect to solvent uptake. The diffusion coefficient for ethyl acetate in PMA is $\sim 10^{-8}$ cm^2/s.[5]

For a reasonable equilibration time, for example, $t \sim 1$s, we use $t \sim \frac{L^2}{D}$ to find $L \sim 1$ μm. Since these films are 10−100× thinner than those employed in typical SANS experiments, we stack 10 of the ~ 1 μm thick films supported on silicon wafers to improve signal-to-noise while assuring equilibration in a reasonable time (the actual mean film thickness was 766 ± 40 nm); we have previously employed this stacking approach for films as thin as 50 nm.[19,20] To controllably expose all films to a vapor stream,[21] we designed a custom titanium flow cell which holds a total of 10 1″ diameter wafers (Figure 1). However,

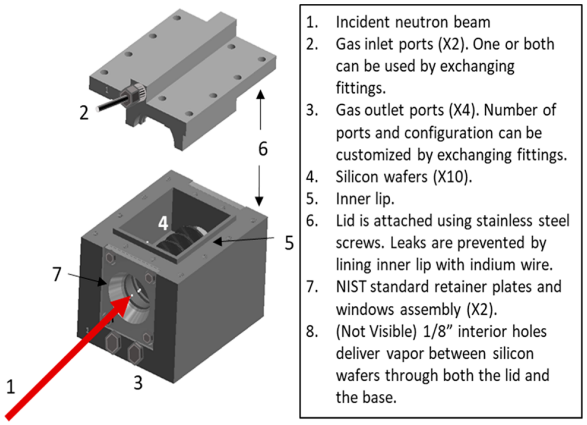

Figure 1. Custom sample holder for SANS swelling experiments. Inlet and outlet ports continue through the cell. Retaining plates, windows, and screws were provided by NIST.

many days of beam time are still required to measure multiple solvent contrast and concentration conditions. Therefore, for this particular study, we limit our investigation to a single GNP architecture near the maximum permeability for EtAC.[5] Details of samples used, film preparation, the vapor handling system, and flow cell are in the Supporting Information.

Figure 2 shows the 1D SAXS intensity as a function of solvent concentration (hydrogenated "EtAC-h$_8$") in the GNP

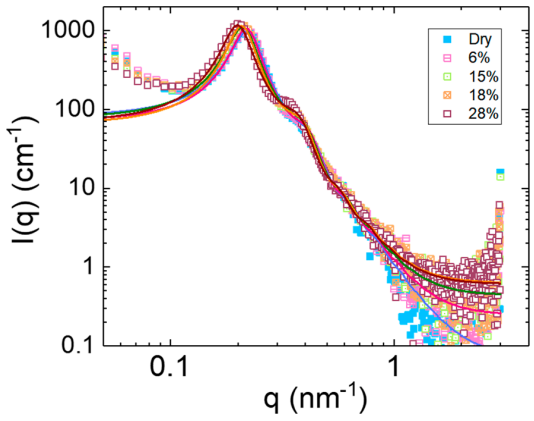

Figure 2. In situ SAXS intensity upon solvent swelling for various solvent concentrations [ϕ_s (V)]. Lines are fit curves.

membrane. With increasing solvent loading, the small angle peak shifts systematically to lower q, i.e., to larger NP spacing. The peak positions of the relative scattering intensities for all solvent concentrations are most closely fit by the hard-sphere model (i.e., the Percus−Yevick[22] structure factor) in combination with a spherical form factor (including a log-normal size distribution of the silica cores with a shape factor, $\Sigma = 0.28$). We provide further justification for the selection of the hard sphere form factor model over other models (e.g., core−shell) in the Supporting Information. The change in interparticle spacing relative to that of the dry film can then be directly calculated from the difference in the hard sphere interaction radii between the wet $R_{HS,w}$ and dry $R_{HS,d}$. The film solvent concentration based on a volumetric argument, ϕ_s (V) is $\phi_s(V) = 1 - (R_{HS,w}/R_{HS,d})^{-3}$ (first column in Table 1). Concurrently, the effective volume fraction of NPs in the wet state is $\phi_{p,w} = \phi_{p,d}\left(\frac{R_{HS,w}}{R_{HS,d}}\right)^{-3}$ (second column, Table 1).

However, to properly fit the data, it is critical to first convert the relative scattering intensity data to absolute intensity by accounting for film thickness increases upon swelling. Since the film is supported and constrained in the plane, solvent swelling manifests only as an increase in thickness without changes in lateral dimensions. Since it is difficult to measure the "wet" thickness, we instead estimate it using $l_w = l_d\left(\frac{R_{HS,w}}{R_{HS,d}}\right)^3$ (third column in Table 1). Note that this change from relative to absolute intensity does not change $R_{HS,w}$, but only shifts the data vertically, thus, only affecting the contrast determined.

The contrast, η, is fit to the absolute intensity with $\phi_{p,w}$ fixed. We can then, alternatively, compute the solvent volume fraction as $\phi_s(\eta) = \frac{S_p - \eta - S_{poly}}{S_s - S_{poly}}$, where S is the scattering length density and the subscripts "p", "s", and "poly" refer to the silica NPs, solvent, and polymer, respectively. In particular, for X-rays we used $S_p = 17.747 \times 10^{10}$ cm^{-2}, $S_{poly} = 11.106 \times 10^{10}$ cm^{-2}, and $S_s = 8.324 \times 10^{10}$ cm^{-2}. The resulting ϕ_s (η) are reported in the last column of Table 1. We find the two means of determining the solvent content in the film to be in good agreement (first vs last column in Table 1). Further, we find the EtAC solubility determined in this manner tracks well with values measured using the quartz crystal microbalance technique[5] and from Fujita et al.[23] (see Supporting Information for details). This gives us additional confidence in the solvent concentrations deduced.

While SAXS therefore gives the solvent loading, SANS with selective labeling is required to determine the location of the solvent molecules relative to the NP core. We used three labeling protocols: (i) Protonated ethyl acetate, EtAC-h$_8$ ($S = 0.5017 \times 10^{10}$ cm^{-2}), (ii) Per-deuterated ethyl acetate, EtAC-d_8 ($S = 5.645 \times 10^{10}$ cm^{-2}), and (iii) a "contrast matched" 46 vol % H:54 vol % D solvent mixture, "EtAC-mix" ($S = 3.282 \times 10^{10}$ cm^{-2}) with scattering length density matched to the silica cores ($S = 3.269 \times 10^{10}$ cm^{-2}) based on the gas pycnometry[5] density of silica, ~ 2.1 g/cm^3). For neutrons, the scattering length density of PMA is 1.345×10^{10} cm^2.

Figure 3 shows the SANS 1D intensities along with fitted curves for various solvent concentrations and contrasts (Table 2). The high-q data are fit with a constant, q-independent background. We note that the high-q limit for the NIST data is limited due to a shadow from neutrons scattered from the detector vacuum chamber windows at the standard 1 m sample

DOI: 10.1021/acsmacrolett.8b00472
ACS Macro Lett. 2018, 7, 1051−1055

Table 1. Fitting Parameters of Swollen Films in SAXS of Varied Solvent Concentrations[a]

ϕ_s (V)	$\phi_{p,w}$	l_w (cm)	core particle radius (nm)	$\eta \times 10^{10}$ (cm^{-2})	$R_{HS,w}$ (nm)	$\phi_{HS,w}$[b]	ϕ_s (η)
0% (dry)	0.102[c]	7.66×10^{-5}[c]	7.01	6.641	14.6[c]	0.41[c]	N/A
6%	0.096	8.14×10^{-5}	7.01	6.814	14.9	0.33	0.06
15%	0.088	8.99×10^{-5}	7.01	7.074	15.4	0.40	0.16
20%	0.082	9.53×10^{-5}	7.01	7.180	15.7	0.41	0.19
28%	0.074	10.66×10^{-5}	7.01	7.448	16.3	0.40	0.29

[a]Core size polydispersity is included using a log normal distribution with a shape factor Σ=0.28. SAXS measurements were performed using a single supported film. [b]$\phi_{HS,w}$ refers to the volume fraction of hard sphere interactions from a Percus−Yevick structure factor [c]Refers to dry state ($\phi_{p,d}$, l_d, $R_{HS,d}$, $\phi_{HS,d}$).

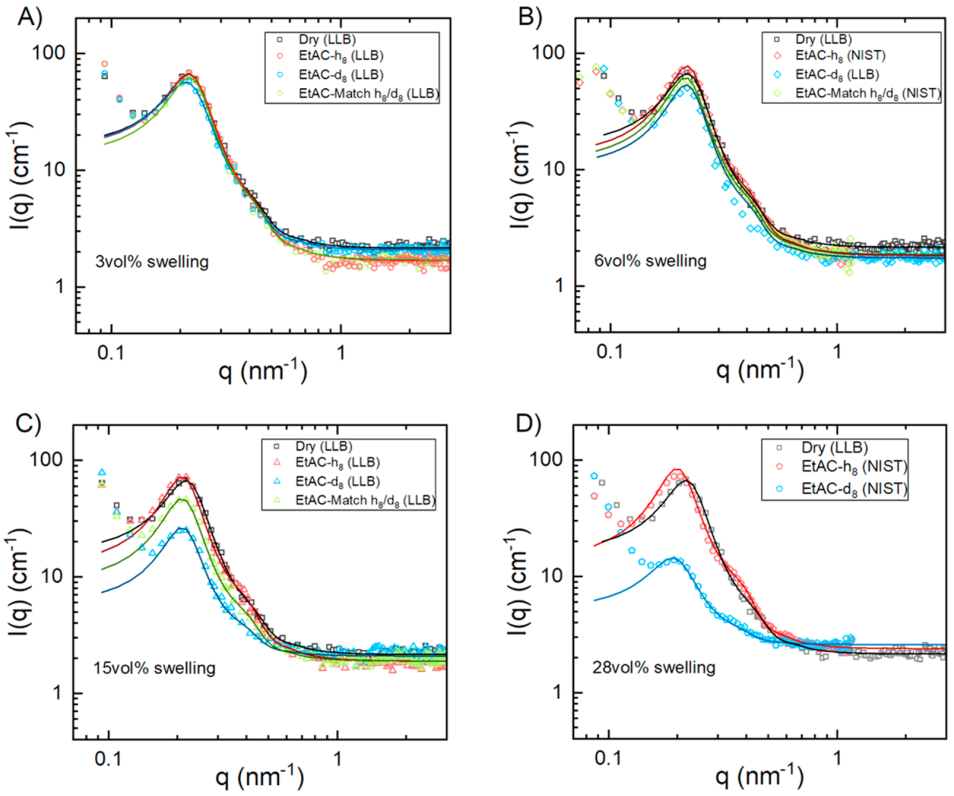

Figure 3. SANS data upon solvent swelling: (A) 3, (B) 6, (C) 15, and (D) 28 vol % solvent with EtAC-h_8 (red), EtAC-d_8 (blue), and EtAC-mix (green). Black curves: dry films (no solvent). Symbols correspond to data and lines to fits. "NIST" indicates data were run on the NG-7 NCNR beamline and "LLB" indicates data were collected on the PA-20 beamline at the LLB.

to detector distance (SDD) used. The smallest SDD for data collected at the LLB was 1.5 m, hence, we obtain a larger usable limit in high-q for these data. At the lowest solvent concentration (3 vol %), there is no obvious change in the low-q peak position; we appear to be below the threshold for determining film swelling. As solvent concentration increases, the main peak shifts to lower q. For these concentrations, the scattering intensity increases with increasing protonated solvent concentration. On the other hand, when we use the mixed solvent or deuterated EtAC-d_8, the low q intensity systematically drops with increased loading; the purely deuterated solvent has the lowest scattering intensity at low q for each concentration. These are surprising results since we expected the "contrast matched" solvent mixture to provide the lowest contrast and, hence, the lowest scattering intensity. They are, however, consistent with the fact that the mean-contrast of the condensed phase is not set by the solvent mixture alone, but rather by a mixture of polymer chains and the solvent. Because of the compositional dominance of the polymer chains (volume fraction >65% in all cases) there is not enough deuterium present, even at the highest concentration of per-deuterated EtAC-d_8, to achieve contrast match conditions. Further, previous work by Higgins suggests that there is hardly any significant chain structure factor contributions in this regime of concentrated polymer solutions.[24,25] These facts suggest that, at all solvent concentrations, the silica cores are surrounded by an essentially homogeneous mixture of solvent and polymer.

Additionally, since the solvent volume fractions obtained from this approach (last column of Table 2 and Supporting Information, Figure S4) are comparable to the SAXS estimates, this method provides a self-consistent check on the assumption that the solvent mixes homogeneously with the polymer brush. Similarly, we do not get satisfactory fits by assuming a core−shell model (i.e., one whose form most closely approximates the theoretical ideas of Daoud and Cotton[8]; Supporting

DOI: 10.1021/acsmacrolett.8b00472
ACS Macro Lett. 2018, 7, 1051−1055

Table 2. Fitting Parameters of Swollen Films in SANS for Various Solvent Concentration Conditions and Solvent Contrast ("solvent type")[a]

ϕ_s (V)	solvent type	beamline	$\phi_{p,w}$	l_w (cm)	core particle radius (nm)	$\eta \times 10^{10}$ (cm^{-2})	$R_{HS,w}$ (nm)	$\phi_{HS,w}$[b]	ϕ_s (η)
0% (dry)	N/A	LLB	0.102[c]	7.66×10^{-4}[c]	7.17	1.921	13.74[c]	0.32[c]	N/A
	N/A	NIST	0.102[c]	7.66×10^{-4}[c]	6.99	1.921	13.80[c]	0.33[c]	N/A
3%	h8	LLB	0.102	7.66×10^{-4}	7.17	1.955	13.73	0.33	0.04
	d8	LLB	0.102	7.66×10^{-4}	7.17	1.775	13.77	0.30	0.035
	mix	LLB	0.101	7.66×10^{-4}	7.17	1.865	13.75	0.32	0.03
6%	h8	NIST	0.095	8.26×10^{-4}	6.99	1.987	14.15	0.34	0.075
	d8	LLB	0.094	8.37×10^{-4}	7.17	1.628	14.15	0.33	0.07
	mix	NIST	0.095	8.12×10^{-4}	6.99	1.815	14.07	0.33	0.06
15%	h8	LLB	0.086	8.91×10^{-4}	7.17	2.063	14.45	0.32	0.17
	d8	LLB	0.086	8.84×10^{-4}	7.17	1.220	14.41	0.32	0.16
	mix	LLB	0.088	8.82×10^{-4}	7.17	1.653	14.40	0.33	0.14
28%	h8	NIST	0.079	10.6×10^{-4}	6.99	2.154	15.40	0.33	0.27
	d8	NIST	0.078	10.1×10^{-4}	6.99	0.870	15.15	0.28	0.245

[a]Core size polydispersity is included using a log normal distribution with a shape factor $\Sigma = 0.28$. SANS measurements were performed by stacking 10 supported films. [b]$\phi_{HS,w}$ refers to the volume fraction of hard sphere interactions obtained from a Percus−Yevick structure factor fir. [c]Refers to dry state ($\phi_{p,d}$, l_d, $R_{HS,d}$, $\phi_{HS,d}$).

Information, Figure S5). Thus, we find that, regardless of solvent concentration or scattering length density, the scattering profiles are best described by a hard sphere form factor with a uniform background comprised of the polymer and solvent.

We therefore conclude the solvent penetrates the entire brush uniformly, even near the NP surface. In parallel work we have found similar results when we considered these same silica NP grafted with PMMA chains (the same grafting density but a higher molecular weight of 100 kg/mol) mixed with a lower molar mass d-PMMA matrix (2.5 kg/mol). While our conclusions are thus consistent with each other, new results with a larger molecular mass PMMA (100 kg/mol) matrix show distinct signs that the matrix chains are excluded from the inner core of the dense brush. These high molecular weight "solvent" results are similar to both scaling theories as well as previous experimental results of GNPs dilute solution, which demonstrate the highly stretched inner regime remains "dry" of solvent.[9,10,26,27] We conjecture that the uniform distribution of a small molecule solvent therefore stems from the incompressibility restriction where the system attempts to maintain a uniform polymer density in the dry state of these (grafted) melts.[6,7] It is surprising, however, that this uniform swelling persists up to relatively high solvent loading near 30%. As of yet, it remains unclear at what solvent concentration the incompressibility condition no longer requires a homogeneous solvent distribution. A logical next step of this work, then, would be to study in-depth the effects of solvent quality and molar mass, as well as the graft density and M_n of the GNPs on the solvent distribution as a function of distance from the nanoparticle surface. Results of such studies may elucidate exactly how the scaling of spherical polymer brushes in the concentrated state (i.e., low solvent loading) may differ from current theories of these materials in dilute solution. In any case, the nonmonotonic enhancement in permeability seen in these GNP-based membranes most likely does not arise solely from an anisotropic solvent distribution. The origin of these remarkable properties is therefore still not understood and is ongoing.

■ ASSOCIATED CONTENT

Supporting Information

The Supporting Information is available free of charge on the ACS Publications website at DOI: 10.1021/acsmacrolett.8b00472.

Experimental methods, sample flow cell design, vapor control apparatus and operation protocol, in situ SAXS control experiment data and fits, validation of solvent concentration calculations in the film and comparisons to literature, simulated effects of form factor on scattering intensity as a function of solvent SLD, comparison of solvent concentration as determined from a volume argument and scattering length density fits, and a sensitivity analysis for the detection of segregated solvent (PDF).

■ AUTHOR INFORMATION

Corresponding Author

*E-mail sk2794@columbia.edu.

ORCID

Eileen Buenning: 0000-0003-1450-1722
Jacques Jestin: 0000-0001-7338-7021
Yucheng Huang: 0000-0002-2367-6199
Brian C. Benicewicz: 0000-0003-4130-1232
Sanat K. Kumar: 0000-0002-6690-2221

Author Contributions

E.B., J.J., B.C.B., C.J.D., and S.K.K. designed the experiments. E.B., J.J., and Y.H. performed experiments. E.B. analyzed the data. The manuscript was written by E.B., J.J., and S.K.K. The project was conceived by S.K.K. and C.J.D. All authors have given approval to the final version of the manuscript.

Notes

The authors declare no competing financial interest.

■ ACKNOWLEDGMENTS

Partial financial support for this work was provided by the National Science Foundation Graduate Research Fellowship Program (E.B.: Grant No. DGE-11-44155) and the NSF DMREF Program (CBET: 1728210). SANS experiments at The Center for High Resolution Neutron Scattering

DOI: 10.1021/acsmacrolett.8b00472
ACS Macro Lett. 2018, 7, 1051−1055

(CHRNS) are jointly funded by the National Science Foundation under Agreement No. DMR-1508249 and by the NIST Center for Neutron Research (NCNR). SANS experiments at the LLB were conducted under Proposal No. 12778. We thank Marc Detrez for his technical support on PA20. SAXS experiments were performed through the South Carolina SAXS Collaborative, supported by the NSF Major Research Instrumentation Program (Award No. DMR-1428620). We thank Dr. Morgan Steffik, Kayla Lantz, and Zackary Marsh for their help with conducting the SAXS experiments. E.B. thanks Dr. Yimin Mao and Dr. Paul Butler for their continuing assistance with the NCNR experiments. E.B. thanks Andrew Jimenez, Sebastian T. Russell, and Connor R. Bilchak for their experimental assistance.

REFERENCES

(1) Kumar, S. K.; Benicewicz, B. C.; Vaia, R. A.; Winey, K. I. 50th Anniversary Perspective: Are Polymer Nanocomposites Practical for Applications? *Macromolecules* **2017**, *50* (3), 714−731.
(2) Akcora, P.; Liu, H.; Kumar, S. K.; Moll, J.; Li, Y.; Benicewicz, B. C.; Schadler, L. S.; Acehan, D.; Panagiotopoulos, A. Z.; Pryamitsyn, V.; et al. Anisotropic Self-Assembly of Spherical Polymer-Grafted Nanoparticles. *Nat. Mater.* **2009**, *8* (4), 354−359.
(3) Goel, V.; Pietrasik, J.; Dong, H.; Sharma, J.; Matyjaszewski, K.; Krishnamoorti, R. Structure of Polymer Tethered Highly Grafted Nanoparticles. *Macromolecules* **2011**, *44* (20), 8129−8135.
(4) Che, J.; Jawaid, A.; Grabowski, C. A.; Yi, Y.-J.; Louis, G. C.; Ramakrishnan, S.; Vaia, R. A. Stability of Polymer Grafted Nanoparticle Monolayers: Impact of Architecture and Polymer−Substrate Interactions on Dewetting. *ACS Macro Lett.* **2016**, *5* (12), 1369−1374.
(5) Bilchak, C. R.; Buenning, E.; Asai, M.; Zhang, K.; Durning, C. J.; Kumar, S. K.; Huang, Y.; Benicewicz, B. C.; Gidley, D. W.; Cheng, S.; et al. Polymer-Grafted Nanoparticle Membranes with Controllable Free Volume. *Macromolecules* **2017**, *50* (18), 7111−7120.
(6) Yu, H. Y.; Koch, D. L. Structure of Solvent-Free Nanoparticle-Organic Hybrid Materials. *Langmuir* **2010**, *26* (22), 16801−16811.
(7) Chremos, A.; Panagiotopoulos, A. Z.; Yu, H. Y.; Koch, D. L. Structure of Solvent-Free Grafted Nanoparticles: Molecular Dynamics and Density-Functional Theory. *J. Chem. Phys.* **2011**, *135* (11), 114901.
(8) Daoud, M.; Cotton, J. P. Star Shaped Polymers: A Model for the Conformation and Its Concentration Dependence. *J. Phys. (Paris)* **1982**, *43* (3), 531−538.
(9) Dukes, D.; Li, Y.; Lewis, S.; Benicewicz, B.; Schadler, L.; Kumar, S. K. Conformational Transitions of Spherical Polymer Brushes: Synthesis, Characterization, and Theory. *Macromolecules* **2010**, *43* (3), 1564−1570.
(10) Ohno, K.; Morinaga, T.; Takeno, S.; Tsujii, Y.; Fukuda, T. Suspensions of Silica Particles Grafted with Concentrated Polymer Brush: A New Family of Colloidal Crystals. *Macromolecules* **2006**, *39* (3), 1245−1249.
(11) Morinaga, T.; Ohno, K.; Tsujii, Y.; Fukuda, T. Structural Analysis of "Semisoft" Colloidal Crystals by Confocal Laser Scanning Microscopy. *Macromolecules* **2008**, *41* (10), 3620−3626.
(12) Cheng, S.; Stevens, M. J.; Grest, G. S. Ordering Nanoparticles with Polymer Brushes. *J. Chem. Phys.* **2017**, *147* (22), 224901.
(13) Baran, L.; Sokolowski, S. Effective Interactions between a Pair of Particles Modified with Tethered Chains. *J. Chem. Phys.* **2017**, *147* (4), 044903.
(14) de Oliveira, O. V.; Costa, L. T.; Leite, E. R. Molecular Modeling of a Polymer Nanocomposite Model in Water and Chloroform Solvents. *Comput. Theor. Chem.* **2016**, *1092*, 52−56.
(15) Nair, N.; Park, M.; Handgraaf, J.-W.; Cassiola, F. M. Coarse-Grained Simulations of Polymer-Grafted Nanoparticles: Structural Stability and Interfacial Behavior. *J. Phys. Chem. B* **2016**, *120* (35), 9523−9539.
(16) Chen, G.; Li, H.; Das, S. Scaling Relationships for Spherical Polymer Brushes Revisited. *J. Phys. Chem. B* **2016**, *120* (23), 5272−5277.
(17) Janes, D. W.; Kim, J. S.; Durning, C. J. Interval Sorption of Alkyl Acetates and Benzenes in Poly(Methyl Acrylate). *Ind. Eng. Chem. Res.* **2013**, *52* (26), 8765−8773.
(18) Orwoll, R. a; Arnold, P. a. Polymer − Solvent Interaction Parameter X. *Phys. Prop. Polym. Handb.* **2007**, *50* (3), 451.
(19) Jones, R.; Kumar, S.; Ho, D.; Briber, R.; Russell, T. Chain Conformation in Ultrathin Polymer Films. *Nature* **1999**, *400* (6740), 146−149.
(20) Shelton, C. K.; Epps, T. H. Block Copolymer Thin Films: Characterizing Nanostructure Evolution with in Situ X-Ray and Neutron Scattering. *Polymer* **2016**, *105*, 545−561.
(21) Shelton, C. K.; Jones, R. L.; Dura, J. A.; Epps, T. H. Tracking Solvent Distribution in Block Polymer Thin Films during Solvent Vapor Annealing with in Situ Neutron Scattering. *Macromolecules* **2016**, *49* (19), 7525−7534.
(22) Wertheim, M. S. Exact Solution of the Percus-Yevick Integral Equation for Hard Spheres. *Phys. Rev. Lett.* **1963**, *10* (8), 321−323.
(23) Fujita, H.; Kishimoto, A.; Matsumoto, K. Concentration and Temperature Dependence of Diffusion Coefficients for Systems Polymethyl Acrylate and N-Akyl Acetates. *Trans. Faraday Soc.* **1960**, *56* (56), 424−437.
(24) Ullman, R.; Benoit, H.; King, J. S. Concentration Effects in Polymer Solutions As Illuminated by Neutron Scattering. *Macromolecules* **1986**, *19* (1), 183−188.
(25) King, J. S.; Boyer, W.; Wignall, G. D.; Ullman, R. Radii of Gyration and Screening Lengths of Polystyrene in Toluene as a Function of Concentration. *Macromolecules* **1985**, *18* (4), 709−718.
(26) Dimitrov, D. I.; Milchev, A.; Binder, K. Polymer Brushes in Solvents of Variable Quality: Molecular Dynamics Simulations Using Explicit Solvent. *J. Chem. Phys.* **2007**, *127* (8), 084905.
(27) Wei, Y.; Xu, Y.; Faraone, A.; Hore, M. J. A. Local Structure and Relaxation Dynamics in the Brush of Polymer- Grafted Silica Nanoparticles. *ACS Macro Lett.* **2018**, *7*, 699.

DOI: 10.1021/acsmacrolett.8b00472
ACS Macro Lett. 2018, 7, 1051−1055